CHEMPHYSCHEM

DOI: 10.1002/cphc.201000069

Quantum-Dot-Sensitized Solar Cells

Sven Rühle,* Menny Shalom, and Arie Zaban*[a]

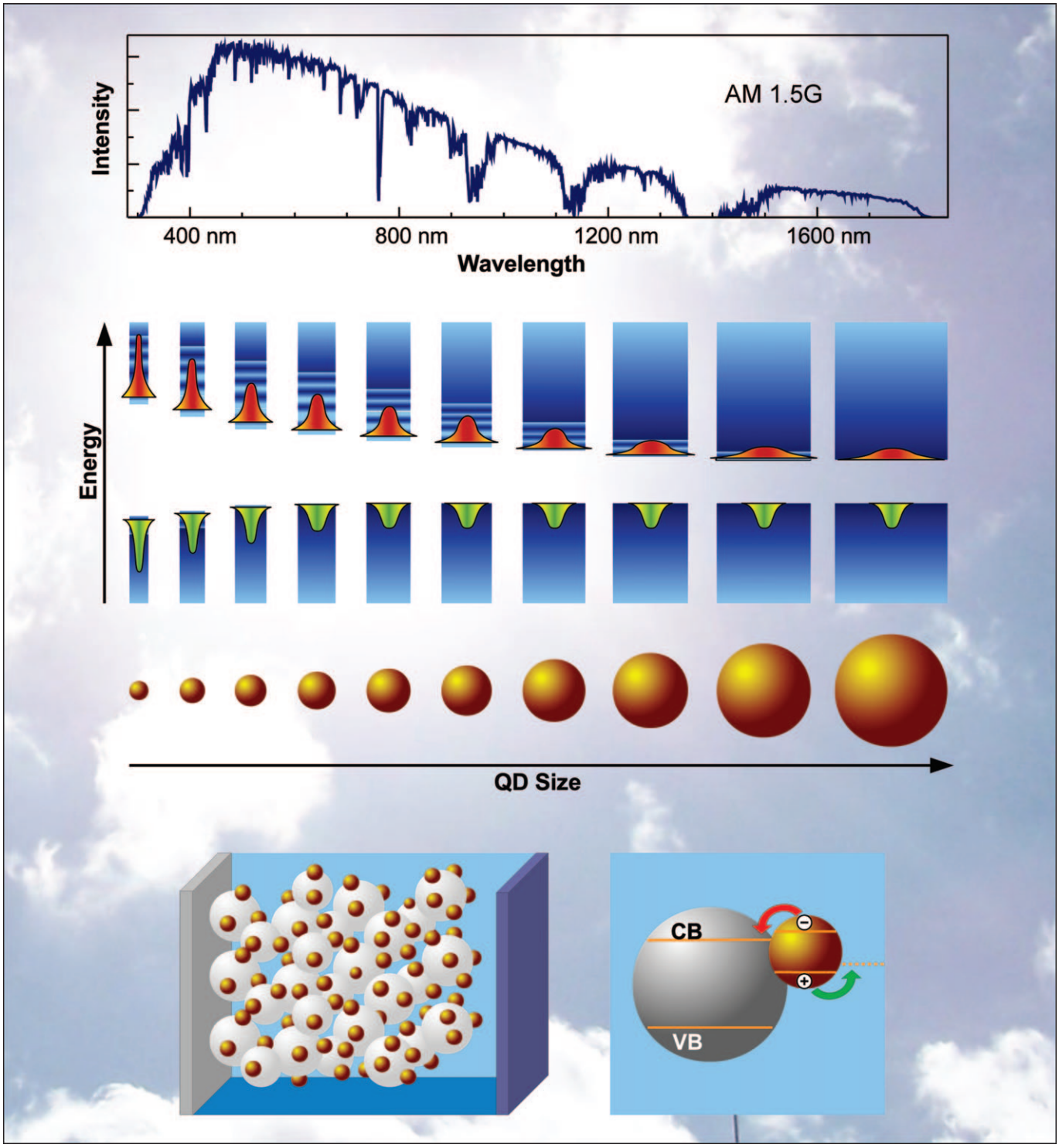

Quantum-dot-sensitized solar cells (QDSCs) are a promising low-cost alternative to existing photovoltaic technologies such as crystalline silicon and thin inorganic films. The absorption spectrum of quantum dots (QDs) can be tailored by controlling their size, and QDs can be produced by low-cost methods. Nanostructures such as mesoporous films, nanorods, nanowires, nanotubes and nanosheets with high microscopic surface area, redox electrolytes and solid-state hole conductors are borrowed from standard dye-sensitized solar cells (DSCs) to fabricate electron conductor/QD monolayer/hole conductor junctions with high optical absorbance. Herein we focus on recent developments in the field of mono- and polydisperse QDSCs. Stability issues are adressed, coating methods are presented, performance is reviewed and special emphasis is given to the importance of energy-level alignment to increase the light to electric power conversion efficiency.

1. Introduction

Limiting the global temperature increase to 2 °C is the biggest challenge of the 21st century. To prevent the collapse of our current climate, greenhouse gas emissions from developed countries must be strongly reduced, while newly industrialized countries must limit increases in CO_2 emissions. To achieve this goal alternative energy sources to coal, oil and gas must be provided, such as power from wind and water, biomass, or solar energy. While a future energy mix will most likely be based on all these sources, only the sun provides our planet with about 10000 times more energy than our global daily consumption. Solar energy can be converted to heat, which can be used directly for warm-water supplies. Higher temperatures can be achieved by light concentration with optical elements like mirrors and lenses, and this provides the opportunity to operate a steam engine and to convert heat into motion and subsequently electricity. The most direct way to convert sunlight into electricity is the use of photovoltaic (PV) cells. PV cells require very little maintenance due to the absence of moving components, and this makes them attractive for long-term outdoor installation.

The PV market has shown exponential growth over the last few years, albeit with a devation from this trend in 2009 due to the global economic crises. Worldwide photovoltaic systems with a total peak power of about 6 GW were newly installed in 2008, which corresponds to five to six conventional coal or nuclear power plants and shows that photovoltaics has left the niche of low-power off-grid applications. Nevertheless, PV electric power cannot compete with the price of electricity from the grid and is therefore supported by national subsidy programs with the aim of reducing the cost of PV systems by increasing production volume. Consequently, further advancement in the research and development of new PV cells is required to increase the light to electric power conversion efficiencies and to reduce prices.

Photovoltaic cells are commonly classified as first-, second- and third-generation devices, depending on the underlying technology. Single- or multicrystalline p–n junction silicon cells are today the most common PV converters with a market share of about 85% and are so-called first-generation devices. High purity requirements for the silicon crystals, high fabrication temperatures and the large amount of material which is needed for a wafer-based cell are major cost factors. Second-generation PV is based on thin films, which are typically deposited between a transparent conducting substrate and a back electrode. Second-generation PV modules have currently a market share of about 15% and are mostly based on CdTe. However, also PV panels based on $CuInS_2$, $CuInSe_2$, $CuInGaSe_2$ or amorphous and nanocrystalline silicon have reached the stage of commercialization and have entered the PV market.

The thermodynamic limit of the light to electric power conversion efficiency η of a single-junction PV cell (1st or 2nd generation) which is optimized to the AM 1.5G spectrum is 32.9%.[1] This limit, also known as Shockley–Queisser limit[2] originates from the fact that photons with energies below the band-gap energy are not absorbed, while photons with energies above the band-gap energy release the additional energy ($E_{photon}-E_{gap}$) mostly as heat. Third-generation solar cells aim towards conversion efficiencies beyond the Shockley–Queisser limit through advanced PV concepts such as multijunction cells, optical up- and downconverters, multiple carrier generation by impact ionization, impurity band cells, and so on. Record conversion efficiencies slightly above 40% have been reported for multijunction cells using concentrated sunlight.[3]

Over the last few years quantum dots (QDs) have attracted widespread attention due to their outstanding opto-electronic properties.[4–12] Their absorption spectrum can be tailored by changing their size,[13–16] which makes them attractive for PV applications. Numerous architectures for QD-based solar cells were proposed including photoelectrochemical cells based on QD-sensitized wide-bandgap nanostructures,[17–19] QD films immersed in electrolyte,[20–22] solid-state cells based on QD/polymer blends[23–25] as well as QD layers sandwiched between electron and hole conductors.[26–29] Nanocomposite solar cells can be easily produced in different shapes and geometries, which allow self light tracking[30] and waveguide integration.[31–33] All these devices are characterized by a single charge-separating junction and belong to the group of second-generation PVs.[34] QD-based devices were also proposed to realize third-generation PVs and to achieve conversion efficiencies beyond the Shockley–Queisser limit. Single-junction PV cells based on QDs absorbers are potential candi-

[a] *Dr. S. Rühle, M. Shalom, Prof. A. Zaban*
Institute for Nanotechnology & Advanced Materials
Department of Chemistry, Bar Ilan University
Ramat Gan 52900 (Israel)
Fax: (+972) 3-738-4053
E-mail: ruhles@mail.biu.ac.il
zabana@mail.biu.ac.il

dates as building blocks in third-generation multijunction devices due to the tunability of the absorption spectrum.

Herein we focus on recent advances in QD-sensitized solar cells based on nanostructured films of a wide-bandgap material sensitized with semiconductor QDs. We review the working principle of dye-sensitized solar cells (DSC) due to conceptual similarities and apply it to QDSCs. An overview on the various QDSC structures and materials is given with a focus on photoelectrochemical and solid-state QDSCs, and the importance of the interface chemistry and physics is emphasized. Experimental strategies to increase the conversion efficiency of QDSCs are presented. Alternative QD-based PV concepts as well as more sophisticated concepts including third-generation PVs are briefly reviewed.

Sven Rühle received his PhD from the Weizmann Institute of Science in Rehovot, Israel, where he studied transport and interface properties of mesoporous TiO_2 films commonly used in dye-sensitized solar cells. For his postdoc he joined the group of Prof. Vanmaekelbergh at the Debye Institute at the University of Utrecht (The Netherlands). Since 2008 he has been working on quantum-dot-sensitized solar cells in the Bar Ilan Center for Nanotechnology & Advanced Materials. Recently he received a EU Marie Curie Fellowship for Career Development.

Menny Shalom completed his undergraduate studies in the Department of Chemistry at Bar Ilan University. During his master thesis he investigated the photostability of quantum dot sensitized solar cells. Following the route of quantum dot absorbers, he is currently conducting his PhD research on fundamental issues concerning energy-level alignment and multi-absorber structures for nanocomposite solar cells.

Arie Zaban earned his B.Sc. in Chemistry (summa cum laude) and a Ph.D. in Electrochemistry (with highest distinction) at Bar-Ilan University (1987–1995). After a two year postdoctoral stint at the US National Renewable Energy Laboratory (Denver, CO), he was appointed to the senior faculty at Bar Ilan, where he is currently a Full Professor of Chemistry and Director of the Bar Ilan Institute for Nanotechnology and Advanced Materials.

2. Working Principles of QD-Based PV Cells

The common feature of QD-based solar cells is quantum confinement of the exciton in the absorber material leading to a size-dependent absorption spectrum. Here we review the working principle of the most common QD-based solar cell configurations such as QDSCs and solar cells with a QD multilayer. QDSCs are based on a nanostructure of a wide-bandgap material that is sensitized with a QD monolayer. Conceptual similarities and differences to dye-sensitized solar cells (DSCs)[35] and extremely thin absorber (ETA) cells[36] are discussed. In layered QD solar cells, on the other hand, the absorber film consists of a QD multilayer, which is located in between electron- and hole-conducting phases. Layered QD solar cells have been realized as photoelectrochemical cells and solid-state devices. In this section we present a broader overview of QD-based solar cells including third-generation devices, while we focus throughout the rest of this review on QDSCs.

2.1. Quantum-Dot-Sensitized Solar Cells

Nanostructured wide-bandgap semiconductor films provide a microscopic surface area, orders of magnitude larger than their geometric area, which can be sensitized with a thin absorber layer of low absorbance. The low optical density of a QD monolayer is compensated by a light path that passes through tens to hundreds of QD monolayers. Dye-sensitized solar cells and ETA cells make use of the same concept, and light to electric power conversion efficiencies above 10% have been reached with DSCs.[3]

Wide-bandgap semiconducting (wbSC) mesoporous films, nanorods, nanowires, nanotubes, nanosheets, and so on have been used as nanostructures. The large microscopic surface area is sensitized with a monolayer of QDs, while a redox electrolyte fills the free space around the nanostructures (Figure 1). The QDs absorb light and inject electrons from their excited

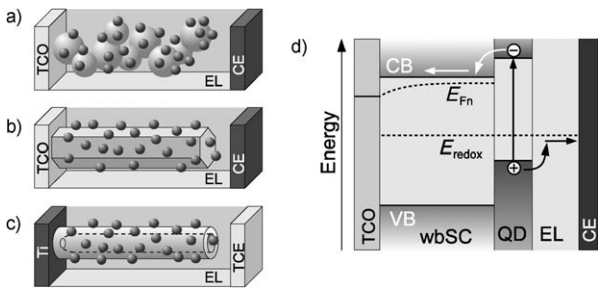

Figure 1. Schematic representation of QDSCs based on a) a mesoporous, wide-bandgap semiconductor film b) nanorods and c) inorganic nanotubes. The QD-sensitized nanostructures are immersed in redox electrolyte (EL), and the circuit is closed by a counter electrode (CE). The latter is usually illuminated through a transparent counter electrode (TCE). d) Energy-band diagram showing the conduction- (CB) and valence-band (VB) edges of the wide-bandgap semiconductor (wbSC), the ground and excited level of the QD and the redox potential E_{redox}. Upon illumination electrons are injected from the excited QD state into the wide-bandgap semiconductor, while the oxidized QD is recharged by the redox electrolyte.

levels into the conduction band (CB) of the wbSC, while oxidized QDs are recharged by the redox electrolyte. Charge transport to the front electrode (usually a transparent conducting oxide, TCO), as well as transport of oxidized redox species to the counter electrode (CE), are diffusion-driven.[37–41]

The absorber thickness in QDSCs, DSCs and also in ETA cells is too small for extended space-charge regions that provide a built-in electrostatic field for charge separation, in contrast to p–n junction solar cells.[42] In particular for DSCs, the working principle has been debated heatedly, especially the question of the electrostatic potential distribution across the device in the dark and under working conditions.[43–51] For DSCs based on mesoporous TiO_2 films in conjunction with an organic electrolyte containing the I^-/I_3^- redox couple, it was shown that band-edge movement of the TiO_2 upon illumination is negligible[52] and that the electrostatic potential changes only in the vicinity of the TCO/TiO_2 interface. Light-induced injection increases the electron concentration in the mesoporous TiO_2 film and leads to an upward shift of the electron quasi-Fermi level E_{Fn} towards the CB edge, while the redox potential E_{redox} remains nearly unperturbed due to the high concentration of redox species typically used in DSCs (Figure 1 d). Under open-circuit conditions electron injection is balanced by recombination, and the energy difference $E_{Fn}-E_{redox}$ determines the open-circuit voltage V_{oc}. For unconcentrated sunlight it was argued that a shift of E_{Fn} into the wbSC CB is unlikely, such that the upper limit of the V_{oc} is determined by the energy difference of the CB edge E_{CB} and E_{redox} of the electrolyte.[53] For DSCs based on mesoporous TiO_2 immersed in organic electrolyte containing I^-/I_3^- an upper limit of about 1.1 eV was estimated, which is significantly higher than the typical photovoltages of 700–800 mV that are observed experimentally. It was pointed out that even at V_{oc} a gradient of E_{Fn} can be present within the mesoporous film due to different recombination kinetics at the TiO_2/electrolyte and FTO/electrolyte interfaces,[54] and recent attempts to cover the FTO surface with wide-bandgap blocking layers support that view.[55,56] For DSCs based on ZnO nanorods it was shown that the doping density can be sufficiently high to generate substantial band bending within larger rods, such that the photovoltage is partly generated by electrons accumulating in the space-charge layer at the nanorod surface.[57]

For QDSCs there has been substantially less discussion regarding their working principle, and many conclusions reached for DSCs are applicable to QDSCs. However, the much wider variety of materials used for QDSCs including aqueous electrolytes, structural differences such as QD coverage of less than a monolayer and the lack of ideal counter electrodes for certain electrolytes must be considered to understand the working principle of a specific QDSC configuration. The pH of aqueous electrolytes shifts the band edges of oxide semiconductors,[58] and thus influences the energy-level alignment. Furthermore, the pH can affect the density of surface traps, and electron accumulation in such states can lead to photoinduced band-edge movement, which is not observed with the organic electrolyte containing I^-/I_3^- in DSCs. Furthermore, the QD coverage of the nanostructured electron conductor can affect the recombination kinetics and subsequently the cell performance. In summary, the main working principle of QDSCs is very similar to DSCs, but further effects such as photoinduced band-edge movement can occur in QDSCs, depending on the composition of the cell material.

For large-scale applications of DSCs and QDSCs it is desirable to replace the liquid electrolyte by a solid-state hole conductor, mainly to reduce difficulties associated with sealing. Additionally, solid-state hole conductors are interesting because the highest photovoltages reported for DSCs were achieved with solid-state devices.[59] The main conceptual difference of solid-state cells is a large recombination current at the TCO/solid hole conductor interface which shunts the device. Compact wbSC layers are required to cover the FTO electrode to prevent recombination. In contrast to nanostructured solar cells based on liquid electrolyte, solid-state cells have only shown good performance in the presence of such a blocking layer.

2.2. QD-Layer-Based Solar Cells

CdSe films deposited from aqueous solutions have shown pronounced size confinement with a blue-shift of the bandgap of around 0.5 eV.[20] Even though the nanocrystals formed a three-dimensional network (shown schematically in Figure 2 a), electronic coupling between them remained sufficiently small to keep excitons size-confined. On immersion in polysulfide electrolyte, photocurrents above 1 mA cm^{-2} and photovoltages of 400 mV were obtained under AM1 illumination. It was argued that the photovoltaic performance originates from preferential hole injection into the electrolyte, leaving behind excess electrons in the film, which are collected at the photoelectrode, while the positive charges diffuse to the counter electrode. An energy-band diagram is presented in Figure 2 b.

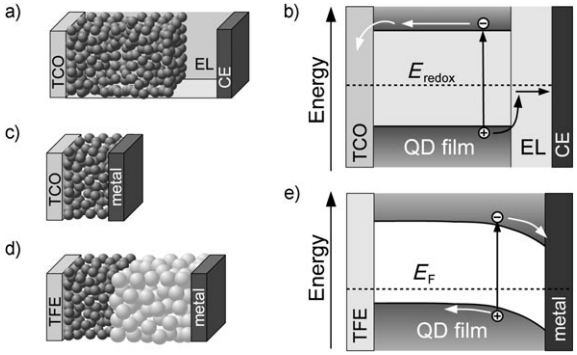

Figure 2. a) Schematic drawing of a photoelectrochemical cell based on a porous QD film immersed in redox electrolyte. b) Energy-band diagram of the device shown in (a). c) Solid-state PV cells based on a thin QD film deposited between a TCO front electrode and a metal back contact. d) Heterojunction cell based on a QD layer and a nanocrystalline wide-bandgap semiconducting layer, sandwiched between a transparent front electrode (TFE) and a metal back electrode. e) Energy-band diagram of the device depicted in (c), showing charge separation at the Schottky junction.

Solid-state PV cells based on thin nanocrystalline films, deposited between a transparent conducting front electrode

(TFE) and metal back-contact were reported.[60,61] However, quantum confinement was only observed in a few cases.[26–29] Figure 2c shows a schematic of a QD layer between asymmetric contacts, while a QD/nanocrystal heterojunction is shown in Figure 2d. It was proposed that such PV cells operate on the basis of a Schottky junction, in contrast to the intermixed three-dimensional junction of the nanocomposite QDSCs discussed above. Charge separation at the Schottky junction is schematically shown in the energy-band diagram depicted in Figure 2e.

2.3. Quantum Dots for Third-Generation Photovoltaics

Advanced methods to bypass the Shockley–Queisser limit include intermediate-band[62,63] and quantum-well solar cells,[64–67] QD-based cells for multi-carrier generation by impact ionization[68,69] and multiple-junction tandem cells.[70] Furthermore, optical methods such as photon up- and downconversion can be utilized.[71] Intermediate-band and quantum-well solar cells can convert photons with sub-bandgap energy into electric energy.[72–74] More precisely, sub-bandgap photons can excite electrons into a sub-band or quantum-well state where they are metastable. The electron can absorb a second photon that excites it into the CB to generate a photovoltage which is higher than the corresponding potentials $\hbar\omega/q$ of the photons absorbed by the cell ($\hbar$ is the Planck constant divided by 2π, ω is photon angular frequency and q the elementary charge). Recently, QDs for multiple exciton generation from a single photon have been studied intensively.[69,75–79] However, until today the results are mostly based on optical measurements, and complete solar cells with incident photon to current efficiencies larger than 100% have so far not been reported to the best of our knowledge. Quantum dots have been proposed as suitable materials to realize photon up- and downconverters. However recent calculations show that this concept can be beneficial only at very high upconversion/downconversion efficiencies and provided that the upconversion/downconversion system does not affect the process in the spectral region of the unmodified photons.[80]

Multijunction tandem cells consist of two or more subcells, each of which is optimized to a certain wavelength range of the solar spectrum.[1,81] QDSCs have great potential for use as subcells in third-generation tandem devices, providing their conversion efficiency is increased dramatically over the next few years. Calculations show that optimized absorption onsets of the individual junctions are critical to achieve high conversion efficiencies with multijunction devices.[1] Quantum confinement provides an easy way to tune the absorption onset, which is very suitable for high-performance multijunction cells. This, however, also requires that the difference between the optical bandgap and the photovoltage must be minimized, for example, in that the electrical energy of a generated electron–hole pair approaches the photon energy at the absorption onset (within the limits of thermodynamics). A three-junction tandem cell based on QDSCs is schematically shown in Figure 3. The absorption of each junction can be tuned by changing the QD size; however, the electron conductor must also be changed to avoid a large energy difference between the QD excited level and the CB of the nanostructure. The individual cells are connected in series by means of intermediate layers consisting of a transparent counter electrode, a recombination layer and a TCO layer onto which the next nanostructure is deposited. Solid-state QDSCs can be more easily stacked together, and sealing problems of different electrolyte compartments can be avoided. Tandem cells have been realized by using two different DSCs physically separated by a glass sheet, and conversion efficiencies above 10% were reported.[70]

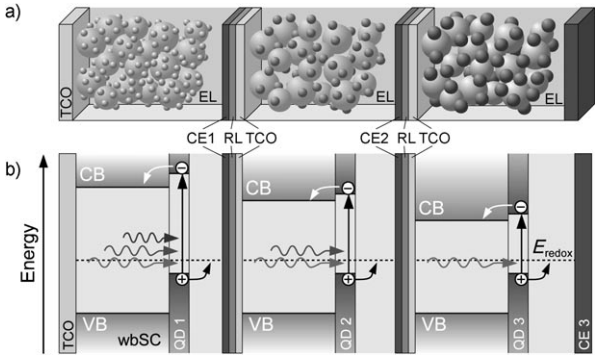

Figure 3. a) Schematic drawing of a three-junction QDSC-based tandem cell. The individual cells are separated by a multilayer stack consisting of a transparent or at least semitransparent counter electrode, a recombination layer and a TCO, which serves as a substrate for the following cell. b) Energy-band diagram, showing the different bandgaps of the QDs and the CB levels of the different wide-bandgap semiconducting nanostructures.

3. QDSC Materials and Synthesis

3.1. QD Materials

Semiconductors such as CdS, CdSe, CdTe, $CuInS_2$, Cu_2S, PbS, PbSe, InP, InAs, Ag_2S, Bi_2S_3 and Sb_2S_3 have been synthesized as QDs and deposited onto wide-bandgap nanostructures as sensitizers. Depending on their size, these materials can absorb photons over a broad spectral range or within a confined window of the solar spectrum. Especially CdS, CdSe and PbS have been used to investigate the operating principles of QDSCs. The limited number of materials listed indicates that much room remains for materials scientists to identify new semiconductors which can be applied as QD sensitizers. Table 1 lists the most common material compositions used for QDSCs. Due to the many publications in latter years, the table only includes a fraction of the work done in this field, in order to highlight articles that contain a detailed description of QD deposition and methods for solar-cell fabrication.

3.2. QD Synthesis and Sensitization

Quantum dot sensitizers can be synthesized by two fundamentally different techniques: in situ and ex situ. Chemical bath deposition (CBD) and successive ionic-layer adsorption and reaction (SILAR) are widely used in situ methods for preparation of QDs on nanostructured wide-bandgap semiconductors

Table 1. QD absorbers used in conjunction with different wide-bandgap semiconductor nanostructures.

Absorber	Deposition method	Electron conductor TiO_2	ZnO	other
CdS	CBD	[82–84][a]	[85][b]	
	SILAR	[17, 86–89][a] [90, 91][c]	[92][a] [93, 94][b]	SnO_2[95]
	linker	[96–98][a]		
CdSe	CBD	[82, 99–102][a]		
	SILAR	[103][a]		
	linker	[99, 104–111][a] [112, 113][c]	[114][a] [115, 116][b]	carbon nanotube[117]
	DA	[99, 113][a]		
CdTe	linker	[107][a] [118][c]	[119][b]	
InAs	linker	[120][a]		
InP	linker	[19][a]		
	CBD	[121][a]		
PdS	SILAR	[87][a]		
	linker	[122][a] [123][c]		
PbSe	linker		[26][a] [124][b]	
$CuInS_2$			[125][b]	
Ag_2S, Bi_2S_3, Sb_2S_3	SILAR	[18][a]	[18][a]	Ta_2O_5[18] Nb_2O_5[18] SnO_2[18]

[a] Mesoporous film. [b] Nanorods. [c] Nanotubes.

which provide high surface coverages of QDs. The in situ approach depends on the nucleation mechanism inside the nanostructure followed by QD growth, which usually leads to a polydisperse QD size distribution. The direct connection between the QD and the wide-bandgap semiconductor leads to efficient charge injection from the QD into the wide-bandgap material. In general higher surface coverages can be achieved with in situ methods.

Pre-synthesized monodisperse QDs, on the other hand, are usually prepared ex situ and are either bound by molecular linkers or deposited directly without linker molecules onto the surface of the wide-bandgap nanostructure (direct adsorption). There are two limiting factors for colloidal QDSCs: first, the chemical nature of the bifunctional molecular linker plays a significant role in charge separation and subsequently in the light to electric power conversion efficiency of the cell.[96, 104–106] Secondly, the surface coverage of QDs on the wide-bandgap nanostructured metal oxide is usually poor when ex situ QD preparation is used.[99] For efficient solar cell operation, strong light absorption followed by efficient charge separation is required, which so far has been more difficult to achieve with QDSCs based on ex situ QD preparation .

3.2.1. Chemical Bath Deposition

Chemical bath deposition has been used to deposit QD films of metal sulfides and selenides onto wide-bandgap semiconductors. Direct growth is done by immersing the wide-bandgap nanostructured electrode (usually a metal oxide) into a solution that contains the cationic and anionic precursors, which react slowly in one bath.[21] For sulfide QDs the CBD technique is often based on the slow release of S^{2-} from thiourea. For selenides Na_2SO_3 is commonly used to reduce selenium to form an Na_2SeO_3 complex which slowly releases Se^{2-} in the presence of metal cations (e.g. Cd^{2+} or Pb^{2+}).

3.2.2. Successive Ionic Layer Adsorption and Reaction

In the SILAR approach dissolved cationic and anionic precursors are in separate vessels. For one deposition cycle the bare nanostructured electrode is dipped into the precursor solution containing the metal cation. After rinsing, the electrode is dipped into the second precursor solution containing the anion, and a second rinsing step completes the deposition cycle. The average QD size can be controlled by the number of deposition cycles. This method has been used in particular to prepare metal sulfides, but recently it was expanded to metal selenides and tellurides.[103]

3.2.3. Monodisperse QDs with Molecular Linkers

Monodisperse QDs are pre-synthesized by using capping agents to control nanocrystal shape, size and subsequently the absorption spectrum and luminescence. Most commonly, synthesis is done in a three-neck flask in which the metal (M) precursor [MO, $M(CH_2)_2$, etc.] is heated to 250–350 °C before an organometallic precursor is injected. Frequently used capping agents are trioctylphosphine (TOP) and trioctylphosphine oxide (TOPO), which dissolve the precursors and prevent aggregation of the QDs. Size is controlled by the temperature and the concentration of the capping agent, and growth can be monitored by UV/Vis spectroscopy. Cooling terminates the growth reaction and can be used to synthesize any desired QD size. After the synthesis of the QDs the metal oxide electrode is immersed in a solution of a bifunctional molecular linker (usually (COOH)–R–SH, where R is the organic core of the linker). The carboxyl group attaches to the nanostructured metal oxide film, while the thiol remains free to connect to the QD. The modified film is immersed in the QD solution (for several hours or days) for adsorption of QDs onto the metal oxide electrodes, which typically involves fractional ligand exchange. Using oleic acid instead of TOPO leads to increased ligand exchange and a higher QD load on the metal oxide.[105] Quantum dot self-assembly has also been used on dispersed TiO_2 crystals, where the photoelectrode was fabricated after QD sensitization by a pressing route.[126]

3.2.4. Direct Adsorption (DA)

Direct adsorption was recently proposed for deposition of monodisperse QDs without molecular linkers to the surface of the metal oxide nanostructure. However only a low surface coverage of approximately 14% was achieved with this method, and the attachment mechanism remained unclear.[113]

3.3. Wide-Bandgap Nanostructures

Mesoporous films, nanorods, nanowires and nanotubes are the most common nanostructures for providing a large microscopic surface area for QD deposition. Mesoporous films consist typically of crystals with a diameter of tens of nanometres which are sintered or pressed together to form a continuous network.[37,38] Mesoporous TiO_2 films have been prepared from paste by screen printing and the doctor blade method[127] or from solution by electrophoretic deposition.[128,129] Large particles with diameters of several tens to hundreds of nanometres were introduced directly into the mesoporous film or as a separate layer to enhance the optical path length by light scattering.[127,130]

Nanorods and nanowires usually have high electron mobilities due to the single-crystalline nature of the rod/wire, while their microscopic surface area is smaller than those of mesoporous films.[131] Nanorods and wires can be grown by low-temperature methods ($<100\,^{\circ}C$) such as chemical[132] or electrochemical[133,134] deposition, while at intermediate temperature ($\sim 500\,^{\circ}C$) nanorod synthesis by spray pyrolysis has been demonstrated.[135] Vapour liquid solid (VLS) growth usually requires high temperatures ($900\,^{\circ}C$) and is therefore not suitable for TCO-covered glass substrates. ZnO is a widely used nanorod/wire material for QDSCs due to its simple preparation methods.

Highly ordered TiO_2 nanotubes have been produced by anodic oxidation of titanium foil[91,136] and used as high surface area, wide-bandgap nanostructures for solar cells. Nanostructures consisting of conducting indium tin oxide (ITO) nanocrystals, coated with a thin conformal TiO_2 layer for improved electron transport, were suggested.[137] Alternative morphologies such as nanocombs,[138] sheets,[139] helices[140] and pillars[141] have been synthesized. However, most of these structures do not provide a groundbreaking advantage over the simple nanorod/wire geometry. In summary, a number of low-cost methods are available to produce nanostructures with strongly enhanced microscopic surface area to deposit thin absorber materials.

3.4. Electrolytes/Hole Conductors

The most common electrolytes used in QDSCs are aqueous polysulfide[20] and organic electrolyte with I^-/I_3^- redox couple,[19] commonly used in DSCs. Besides, the Fe^{3+}/Fe^{2+} and the $Fe(CN)_6^{3-}/Fe(CN)_6^{4-}$ redox systems, both in aqueous solution, have been investigated in conjunction with CdS-sensitized cells.[142] Recently a cobalt complex redox couple was proposed in conjunction with CdSe, PbS and CdS sensitized cells.[89,143] Solid-state hole conductors such as spiro-OMeDAT and CuSCN have been used to replace the liquid electrolyte. The performance of the electrolytes and solid-state hole conductors and their advantages and disadvantages are discussed in Sections 4.3 and 5.1, respectively.

3.5. Counter Electrodes

Platinized TCO layers have been used in conjunction with all of the redox electrolytes mentioned above. For the polysulfide electrolyte the Pt counter electrode leads to a rather low fill factor and Au has been used alternatively.[113,144] Hodes et al. investigated metal sulfides (especially Co, Cu and Pb) as suitable counter-electrode materials, measured their long-term stability and pointed out that Cu_2S and CoS may poison the surface of the photoelectrode.[145]

4. QDSC Interfaces

4.1. QD/Wide-Bandgap Nanostructure Interface

4.1.1. Monodisperse QD Sensitizers

The first reported solar cell using pre-synthesized QDs was based on InP QDs attached to mesoporous TiO_2.[19] Since then a number of other QD materials have been used to sensitize wide-bandgap nanostructures (see Table 1). Monodisperse QDs are connected through linker molecules to the nanostructured electron conductor, but electron injection from the excited QD state is in most cases less efficient compared to directly deposited QDs.

The major advantage of monodisperse QD sensitizers is the tuning capability of the absorption onset, which is shown in Figure 4a for CdTe QDs in solution. The increase in the optical bandgap is caused by confinement of the electron and hole wavefunctions. Due to the lower effective mass the electron wavefunction is more spread in space, and electron confinement starts to occur at larger particle diameters than hole confinement. Figure 4b shows schematically wavefunction confinement, the associated splitting of the bands into discrete

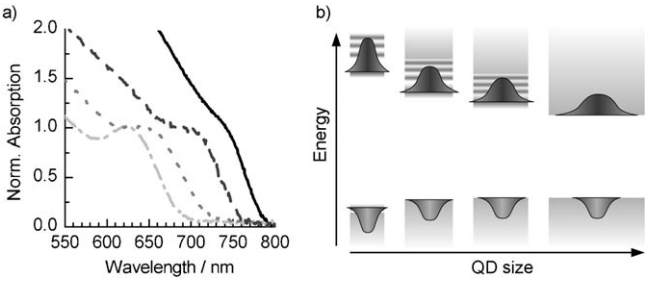

Figure 4. a) Absorption spectra of monodisperse CdTe QDs in solution. The absorption onset shifts towards shorter wavelengths with decreasing QD size. All spectra have been normalized to the first absorption peak. b) Energy-band diagram of a semiconducting nanoparticle, showing decreasing particle size from right to left. Initially only the electron wavefunction is confined before the hole wavefunction is affected. As a result the continuum of electronic states at the band edges breaks up into discrete levels and the bandgap increases.

energy levels and an increase in the bandgap. Experimentally, the correlation between the absorption onset and the photocurrent was presented,[112] emphasizing the potential of QDSCs as building blocks for series-connected third-generation tandem or multijunction cells, in which current matching is critical.

It was shown that the nature of the linker molecule between the QD and the semiconductor nanostructure is critical for operation of the solar cell.[106] Bisquert et al. showed a major improvement of the incident photon to current efficiency (IPCE) and the total photocurrent by changing the linker molecule from mercaptopropionic acid (MPA) to cysteine.[104]

4.1.2. Polydisperse QDs (Deposited in situ)

The absorption onset of polydisperse QDs deposited by CBD or SILAR can be controlled by the growth time or the number of deposition cycles (Figure 5), respectively. In contrast to monodisperse QDs the onset occurs over a broader spectral range and is featureless.

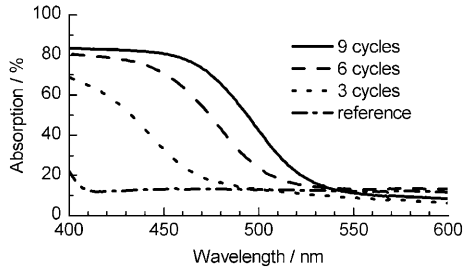

Figure 5. Absorption spectrum of mesoporous TiO_2 electrodes sensitized with CdS QDs by using SILAR. The reference measurement on a mesoporous film shows that 12–15% of the light is reflected or scattered. One deposition cycle consists of dipping the film into 0.1 M $Cd(ClO_4)_2$, rinsing it with distilled water, dipping it into 0.1 M Na_2S and rinsing the film again.

SILAR and CBD are simple and convenient sensitization methods, especially for sulfide and selenide QDs. Often SILAR leads to a higher surface coverage compared to CBD, resulting in higher photocurrents. Charge separation at the electron conductor/QD interface is more efficient than in linker-bound QD deposition. Hodes et al. showed that in CdSe-sensitized TiO_2 electrodes a thin intermediate layer of CdS dramatically improves all solar-cell parameters.[82]

4.2. QD/Electrolyte Interface and Photochemical Stability

The number of redox electrolytes used in QDSCs is limited, even though electrochemistry textbooks contain long tables of redox couples with their respective redox potentials. One reason is the requirement for efficient hole extraction from the QD to prevent recombination and degradation. The most common examples are I^-/I_3^- and polysulfide, whereby the latter shows superior properties in conjunction with sulfide QDs, but its redox chemistry is complex, and it remains challenging to prepare counter electrodes without significant losses due to high charge-transfer resistances.[145]

Current–voltage (*I–V*) measurements on QDSCs with a polysulfide electrolyte generally show a rather low fill factor,[104] while the I^-/I_3^- couple can be used in conjunction with a Pt counter electrode without significant voltage losses. However, the presence of iodine often causes photocorrosion of the QDs.[83,84,146,147] A typical example is shown in Figure 6b, where

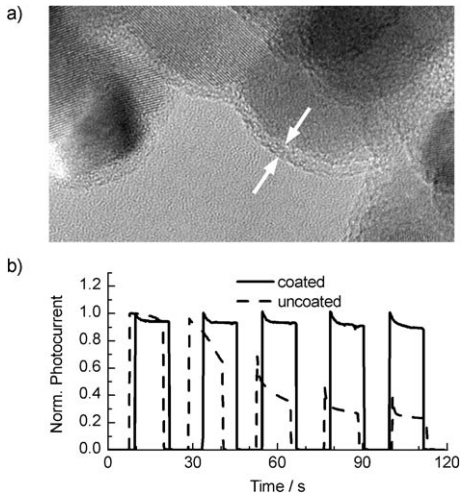

Figure 6. a) High-resolution transmission electron microscopy (HRTEM) image of a mesoporous film consisting of TiO_2 nanocrystals, covered with an amorphous conformal Nb_2O_5 shell by electrophoretic deposition. b) Normalized short-circuit current as a function of time for an amorphous TiO_2-coated and uncoated CdS QD-sensitized electrode with I^-/I_3^- redox electrolyte. The light was periodically switched on and off in intervals of 12 s.

the photocurrent of a CdS-sensitized TiO_2 film without further treatment decays after about 30 s due to photocorrosion. Under such conditions it is not possible to record reliable *I–V* curves. Besides I^-/I_3^- and polysulfide, Kuwabata et al. used the Fe^{3+}/Fe^{2+} and $Fe(CN)_6^{3-}/Fe(CN)_6^{4-}$ redox couples together with a Pt counter electrode in a cell sensitized with CdS QDs.[142] For the I^-/I_3^- and Fe^{3+}/Fe^{2+} redox couples a pronounced incident photon to current (IPC) signal was only recorded below 400 nm, where TiO_2 absorbs, and this is evidence that photocorrosion damaged the QD absorber. With the $Fe(CN)_6^{3-}/Fe(CN)_6^{4-}$ couple a broad IPCE response was observed, similar to QDSCs with a polysulfide electrolyte; however, a compact blocking layer at the TCO/electrolyte interface was required for this redox couple due to efficient electron transfer from the TCO to the electrolyte.[148] Recently, a cobalt complex was used as redox couple in conjunction with a platinized counter electrode to perform stable and reproducible *I–V* measurements on PbS-, CdS- and CdSe-sensitized cells.[89,143] However, this electrolyte suffers from slow ion conductivity which allows efficient operation only under low light intensities. Unlike DSCs, for which an ideal redox system for the dye has been found, no such electrolyte has been identified for QDSCs, and further research in this direction is needed.

4.3. QD/Solid-State Hole Conductor Interface

Mesoporous TiO_2 films sensitized with PbS,[87,121,122] CdS[87,149] or CdSe[103] QDs have been used in conjunction with solid-state hole conductors such as spiro-OMeTAD[87,103,121] and CuSCN.[149] Long-term sealing of solid-state PV cells is much easier compared to photoelectrochemical cells containing liquid electrolyte, and this makes solid-state hole conductors attractive for QDSC applications. Furthermore, it was shown for DSCs that much higher photovoltages can be achieved by using solid-state hole conductors such as spiro-OMeDAT.[59] A major problem of solid-state hole conductors is penetration into the QD-sensitized nanostructured film, which limits the thickness of the mesoporous film and can lead to incomplete photon absorption. In solid-state QDSCs this problem is less pronounced due to the larger absorbance of QD monolayers compared to metal–organic dyes. Until now most of the research on solid-state hole conductors has been carried out on DSCs[150–159] or ETA cells.[160–164] However, research on solid-state QDSCs has recently attracted more attention, and most of the results from DSCs and ETA are likely applicable to nanostructured QDSCs, so that further developments and improvements can be expected.

4.4. Protective Coatings

The low stability of QDs in corrosive electrolytes, recombination by surface traps and the need for enhanced hole extraction from the QD have motivated research to passivate the QD surface in contact with the electrolyte. Inorganic amorphous coatings can be deposited in a conformal and continuous fashion onto mesoporous TiO_2 electrodes (Figure 6a), and for DSCs it was shown that coatings can improve solar cell performance.[165,166] Stable and reproducible *I–V* measurements on using the corrosive I^-/I_3^- redox couple were reported when CdS-sensitized mesoporous TiO_2 electrodes were coated with an amorphous TiO_2 shell by electrophoretic deposition.[146] Photocurrent measurements under periodically switched light for a coated and uncoated electrode (Figure 6b) demonstrate that inorganic coatings can be used to drastically improve the stability of CdS QDs. Conversion efficiencies above 1% were recorded, even though the valence band edge of amorphous TiO_2 should create a barrier for hole injection into the electrolyte.

A dramatic improvement in photocurrent and conversion efficiency was reported for CdSe QDSCs when the sensitized mesoporous TiO_2 electrode was covered with a ZnS shell by dip coating.[100,167] Toyoda et al. showed that the ZnS coating almost doubled the conversion efficiency from 1.12% to 2.02% when using polysulfide electrolyte, which was attributed to passivation of CdSe surface states that trap photoexcited electrons and holes. It was furthermore argued that the ZnS coating creates a barrier for electron injection from the QD into the electrolyte. Considering the valence band level of ZnS, this should also create a barrier for hole transfer into the electrolyte, similar to amorphous TiO_2 coatings. Note that the electronic structure of the coating may differ significantly from that of bulk material due to the very low thickness in the angstrom/nanometre regime. The recent advances in chemical stability and solar cell performance due to the use of coatings are encouraging, and further research is needed to better understand the interface energetics and kinetics.

5. Energy-Level Alignment

Energy levels in QDSCs are always aligned with respect to the adjacent materials. The advantage of QDSCs is the small dimensions of its components, which enable level alignment based on interface dipoles. The wide-bandgap nanostructure and the QDs are usually too small to accommodate significant band bending, so that electronic properties of the bulk material do not dominate the system.

5.1. Conduction-Band Energy-Level Alignment

The photovoltage in electrochemical QD-sensitized solar cells is limited by the energy difference between the CB edge of the electron-conducting nanostructure and the redox potential of the electrolyte, analogous to DSCs. In solid-state cells the CB edge of the electron conductor and the VB edge of the hole conductor limit the photovoltage. For DSCs it was shown that V_{oc} can be shifted in a systematic fashion when molecular dipoles are co-grafted with the dye molecules onto the surface of the mesoporous film.[168–170] This was attributed to a shift of the TiO_2 CB edge with respect to the redox potential. Figure 7 schematically depicts the TiO_2/dye & dipole/electrolyte interface for molecular dipoles pointing away and towards the surface. The related shift of the TiO_2 energy levels is schematically shown in the energy-band diagrams. A similar systematic change of the photovoltage was found when the Li^+ cation of the electrolyte was replaced by Na^+, K^+, Rb^+ or Cs^+.[171] This

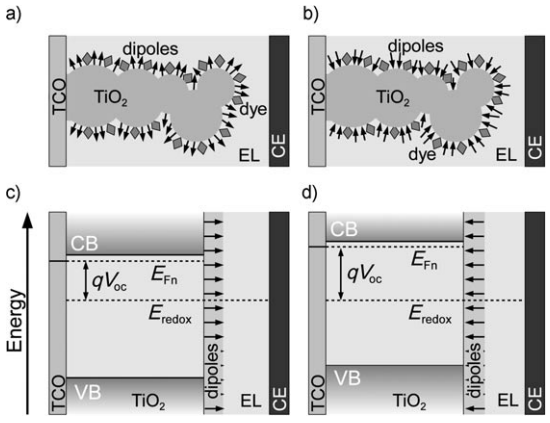

Figure 7. a) Schematic drawing of a mesoporous TiO_2 film covered with a monolayer of dye molecules together with co-adsorbed dipole molecules. The direction of the dipole moment is symbolized by an arrow pointing towards the electrolyte. b) As in a) but with co-adsorbed molecules with dipole moments of opposite direction. c) Energy-band diagram showing the dipole-induced downward shift of the TiO_2 CB with respect to the redox potential and its impact on the photovoltage. d) As in c) but with dipole molecules shifting the TiO_2 levels upwards, such that an increased photovoltage is achieved.

was explained by the different ionic radii and the subsequent potential drop across the Helmholtz layer at the TiO_2/dye/electrolyte interface. Furthermore in oxide semiconductors the band-edge potential can strongly shift as a function of the surface pH.[58] This is of particular importance in photoelectrochemical QDSCs with aqueous electrolytes, in which a fraction of the oxide nanostructured surface is in direct contact with the electrolyte due to incomplete QD surface coverage. Surface pH effects on the photovoltage have also been reported for DSCs with organic electrolytes.[172]

The nanocrystalline oxide/electrolyte interface plays a major role for energy-level alignment in QDSCs and DSCs. Changing the chemical environment at this interface by grafting or co-grafting molecular dipoles, altering the surface pH or varying the electrolyte composition (without changing its redox potential) opens a path for systematic energy-level engineering. As a result, recombination kinetics, charge accumulation and the electrostatic potential drop across the Helmholtz layer are affected and result in a change in the photovoltage.[52] Alignment of the conduction-band level has not received much attention in QD-sensitized solar cells and most of the research has been carried out on DSCs. These methods can be applied to linker bound and in situ deposited QD-sensitized electrodes, and thus provide new possibilities to enhance their performance.

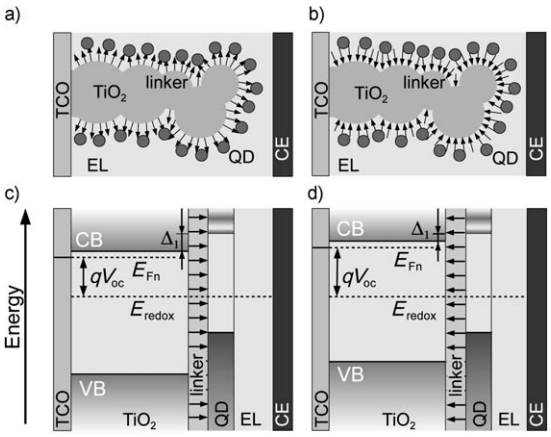

Figure 8. a) Schematic drawing of a mesoporous TiO_2 film, covered with linker molecules with a molecular dipole pointing towards the QD monolayer. b) As in a) but for linker molecules with a dipole pointing in the opposite direction. c) Energy-band diagram showing a downward shift of the energy levels of the wide-bandgap nanostructure due to the dipole moment. d) As in c) but with linker molecules with a dipole moment pointing away from the QDs. As a result the TiO_2 energy bands are shifted towards the vacuum level, which reduces the potential loss at the TiO_2/QD interface (Δ_1) and subsequently increases the open-circuit voltage.

5.2. Quantum-Dot Energy-Level Alignment

Controlling quantum size confinement in monodisperse QDs is the most obvious method to align the energy levels with respect to the wide-bandgap nanostructure.[112] Usually, the electron wavefunction is less localized than the hole wavefunction, so that the electron levels are more strongly affected in the quantum-confinement regime. This effect is schematically depicted in the frontispiece of this review, which shows initially an upward shift of the electron energy levels (towards the vacuum level) with decreasing particle size, while the hole levels remain unaffected. Reducing the size further leads to an additional downward shift of the hole levels, which can be used to optimize the energetics between the QDs and the electrolyte or solid-state hole conductor. The method of quantum confinement for energy-level alignment is limited because it does not permit electron and hole levels to be shifted simultaneously in the same direction.

Surface modification by dipoles provides a simple and efficient way to shift the QD energy levels. For monodisperse QDs it was shown that fractional exchange of the capping ligands by molecular dipoles can be used to shift the electronic QD states with respect to their environment in a systematic fashion.[173]

In linker-bound QDSCs the nature of the molecular linker can be modified to insert a dipole between the QD and the nanostructure. Figure 8 schematically shows the dipole linker covering the nanostructure and connecting the QD to the surface, together with the respective energy-band diagram. Linker molecules bear COOH and SH groups, which bind to the nanostructured oxide and the QD, respectively. The two groups are separated by an organic spacer, which can be modified to change the molecular dipole moment of the linker, although the tuning options are more restricted than for dipoles with only one binding group. Experimentally, it was demonstrated that the type of linker molecule has a strong impact on electron injection from the QD into the nanostructure and on QDSC performance.[104,174]

An alternative method to adjust the QD energy levels with respect to the semiconducting nanostructure was presented recently, whereby the surface of polydisperse QDs prepared in situ was modified with benzenethiol derivatives (Figure 9).[175] The onset of the photoresponse shifted linearly as a function

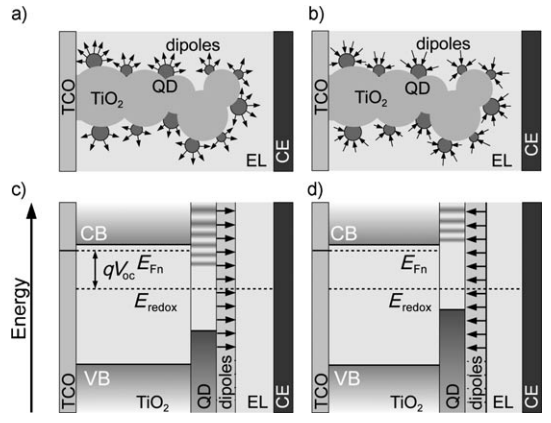

Figure 9. a) Schematic drawing of polydisperse QDs prepared in situ on a mesoporous wide-bandgap semiconductor. Molecular dipoles are only adsorbed at the QD surface. b) As in a) but with dipoles pointing in the opposite direction. c) Energy-level diagram showing the lowest excited QD level for a number of QDs of different size. d) Molecular dipoles shift the QD levels upwards towards the vacuum level such that more QDs can be injected from their lowest excited level into the TiO_2 nanostructure.

of the molecular dipole moment, even though the molecular modification was carried out at the QD/electrolyte interface. This was explained by a dipole-related electric field induced across the QD. Due to the SH binding group of the dipole molecule it was possible to modify specifically the QD surface without affecting the wide-bandgap oxide.

5.3. Hole-Conductor Energy-Level Alignment

In photoelectrochemical cells the redox potential can be aligned by changing the concentration ratio of the reduced and oxidized species according to the Nernst equation. Concentration changes additionally affect the charge-transfer kinetics at the QD/electrolyte interface, which limits the degree of alignment. Specific adsorption of counter ions at the surface of the QDs and/or wide-bandgap nanostructure influences the potential drop at the interface with the electrolyte and can in general be used align energy levels. Especially for solid state DSCs, it was shown that the addition of ionic species to spiro-OMeDAT can have a strong positive impact on the photovoltage.[59]

6. QDSC Performance

6.1. Incident Photon to Current Efficiency

Critical for high light to electric power conversion efficiency in QDSCs are efficient charge separation at the absorber and subsequent collection at the front and back electrodes. The incident photon to current efficiency (IPCE) measures the ratio of charge carriers collected at the electrodes to the number of incident photons, which is also known as external quantum efficiency (EQE). Encouraging IPCE values have been reported for QDSCs, which sometimes show EQEs of 40% or higher over a broad spectral range.[113] For an ideal solar cell the short-circuit current density J_{sc} can be calculated from IPCE data together with the standard AM 1.5G spectrum (Figure 10a). For QDSCs the calculated J_{sc} and the measured J_{sc} under 1 sun (100 mW cm^{-2}; Figure 10b) differ in most cases significantly, that is, QDSCs are not ideal. This is further supported by measurements of conversion efficiency, which show higher η at low light intensities. Measurements of IPCE are often performed without bias light at low monochromatic light intensities, where charge separation and collection are apparently more efficient than at high illumination intensities,[106] and this explains the discrepancy between calculation and direct measurement. Especially hole extraction and charge transport through the electrolyte seem to be limited at illumination intensities approaching 1 sun. To overcome this limitation the charge-transfer kinetics at the QD/electrolyte interface and charge transport through the electrolyte must be improved.

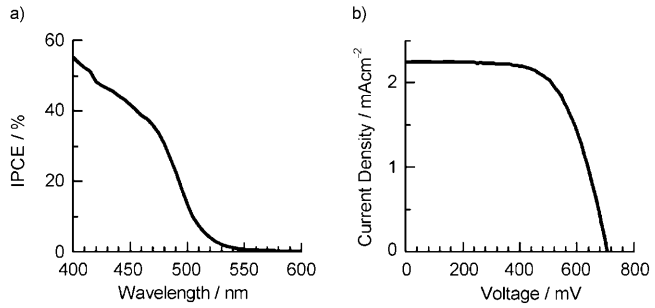

Figure 10. a) IPCE of a CdS QD sensitized mesoporous TiO_2 film, coated with an amorphous TiO_2 layer and measured with an organic electrolyte containing the I^-/I_3^- redox couple. For the AM 1.5G spectrum a short-circuit density of 2.1 mA cm$^-$ is calculated. b) Current–voltage characteristic of the same electrode, showing good correlation between the calculated and measured J_{sc}, which indicates that the coated electrode shows nearly ideal behaviour.

6.2. Light to Electric Power Conversion Efficiency

Reporting light to electric power conversion efficiencies of photoelectrochemical QD-sensitized solar cells is of importance to monitor progress in the field. To enable a meaningful comparison of measurements performed in different laboratories around the world, certain standard conditions should be met. Certain standards have been established to enter the solar cell efficiency tables,[3] which are updated twice per year and strict measurement procedures must be followed. Laboratory cells must be at least 1 cm^2 in size, and measurements must be performed in one of the recognized test centres worldwide. This is of course not practical for every measurement reported in the literature, but some minimum standards should be kept to enable comparison of results from different groups. The cell size should be sufficiently large to minimize edge effects, and *I–V* measurements should be performed with a class A solar simulator that produces a spectrum close to the AM 1.5G standard spectrum with a light intensity of 100 mW cm^{-2}. Thus far record efficiencies close to 4.5% were measured on cells with an area significantly smaller than 1 cm^2 and/or at illumination intensities far below 1 sun.[144] These values are still far below the theoretical limit for QDSCs.

6.3. Three-Electrode Measurements

Recently, several publications reported photocurrents, photovoltages and conversion efficiencies based on incorrect data analysis. The error occurred when a three-electrode system was used and *I–V* data were reported and analyzed versus the reference potential of the reference electrode (for example Ag/AgCl or SCE) and not with respect to the respective dark potential. Consequently, photovoltages significantly higher than 1 V, photocurrent densities up to 16 mA cm^{-2} and conversion efficiencies greater than 4% were erroneously reported. Three-electrode measurements can be used to characterize one of the electrodes (photoelectrode or counter electrode), by separating it from the other components of the cell. In polysulfide-based QDSCs, where a significant part of the photopotential is needed to overcome the charge-transfer resistance at the electrolyte/counter electrode interface, three-electrode measurements can provide useful information about the operation of the sensitized photoelectrode. It is suggested that, besides three-electrode cell analysis, the photovoltaic performance should be measured independently by a two-electrode set-up.

The latter is the easiest way to avoid mistakes associated with the conversion of three-electrode measurements to full-cell *I–V* characteristics.

6.4. Efficiency Limit of QDSCs

The theoretical conversion efficiency limit of a solar cell depends on the optical bandgap of the absorber and the band alignment within the device, providing charge separation and transport are efficient and recombination is suppressed. To reach high conversion efficiencies the difference between the electrical energy of a photogenerated charge (qV_{ph}) and the photon energy at the absorption onset ($\hbar\omega_{onset}$) must be minimized. The energy-band diagram of a QDSC shown in Figure 11a depicts schematically the photon energy $\hbar\omega_{onset}$, the

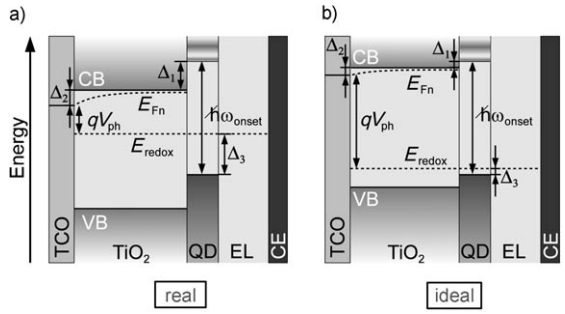

Figure 11. a) Energy-level diagram of a QD-sensitized solar cell showing the energy offset between the excited QD level and the CB edge of the electron conductor (Δ_1), the potential loss associated with the driving force for electron transport (Δ_2) and the energy difference between the oxidized QD level and the redox potential (Δ_3). The total energy loss corresponds to the difference in the photon energy at the absorption onset $\hbar\omega_{onset}$ and the electrical energy qV_{ph}. b) Ideal energy-band diagram with minimized losses Δ_1, Δ_2 and Δ_3.

electrical energy qV_{ph} and the losses Δ_1, Δ_2 and Δ_3 due to non-optimized energy level alignment and transport. The loss in potential Δ of a solar cell can be defined as the sum of the individual losses Δ_i, and minimizing Δ is of paramount importance to increasing the conversion efficiency of solar cells. Figure 6b shows a strongly increased photovoltage V_{ph} when all Δ_i are reduced to the extent that they still generate sufficient driving force for charge separation and transport. The impact of the loss in potential was recently quantified for DSCs, and it was pointed out that a reduction of Δ from 0.75 to 0.4 eV pushes the theoretical conversion efficiency limit from 13.4% to 20.3%, provided that optimized dyes are used in both cases.[176] Similar considerations apply to QDSCs, that is, high conversion efficiencies in the 15–20% range are realistic when the addressed problems can be solved.

Future high-efficiency QDSCs require smart material selection to provide the desired low-loss energy-level architecture. Additionally, methods must be developed which enable systematic energy-level alignment between absorber, electron and hole-conducting phase, for example, the dipole alignment shown above. Band offsets must be reduced to the extent that only the driving force for charge separation is maintained, while thermalization effects must be minimized. If this can be realized, QD-sensitized solar cells will offer a low-cost alternative as building blocks in multijunction third-generation PV cells as well as for broadband single-junction PV devices.

7. Summary

Photovoltaic cells based on QD absorbers were reviewed with the emphasis on QDSCs, based on a wide-bandgap nanostructured electron conductor covered with a monolayer of QDs. Quantum dots have attracted considerable attention for PV applications due to their perfect crystallinity and unique optoelectronic properties, which are defined by the particle size and can be controlled by the growth process. Monodisperse QDs with their characteristic sharp absorption onset are excellent candidates as absorber materials in multijunction third-generation PV cells. Fine-tuning of the absorption spectrum is critical in two terminal devices where current matching of the subcells is required. Upscaling of QD production volume is possible at rather low cost because the wet chemical synthesis does not involve expensive process steps such as high vacuum.

Although the choice of suitable material compositions in QDSCs is important, we emphasize that good control over the interface processes is critical for device operation and improvement. We have shown that alignment of energy-band levels is required to improve the photovoltage and subsequently the conversion efficiency. Molecular modification of the individual interfaces was presented as a possible tool. The QD/electrolyte interface is furthermore affected by the redox chemistry, and the polysulfide electrolyte has shown good performance in conjunction with most QDs. However until now it has not been possible to identify counter electrodes for polysulfide which show satisfactory long-term stability and good performance. The I^-/I_3^- redox couple, on the other hand, shows outstanding performance in DSCs and has been applied to QDSCs, but with limited success due to photodegradation of the QDs in the presence of very corrosive iodine. Alternative redox systems are under investigation.

8. Outlook

The limited number of semiconducting QDs that have been synthesized up to now leaves the field wide open for materials scientists to identify new semiconducting absorbers. Also the very limited number of liquid redox electrolytes that have been investigated in conjunction with QDSCs demonstrates the need for further research. In the long term it is desirable to replace the liquid electrolyte by solid-state hole conductors, and materials known from solid-state DSC and ETA cells have been successfully applied to QDSC. However, these are initial results, and further research is needed to improve solid-state QDSCs. Improving the light to electric power conversion efficiency in QDSCs is critical and requires that the difference between the absorption onset of the QDs and the photovoltage be minimized. As discussed throughout this review, the interface properties within the device are critical for its operation,

and a fundamental understanding of how to control and engineer their properties is lacking. Research in this direction using interface dipoles and coating layers has just started, and further progress is expected in the near future. New methods for energy-level alignment should boost the QDSC efficiency to compete with the conversion efficiency of 15–20%, typical for polycrystalline silicon, but at a significant lower cost.

Acknowledgements

S.R. acknowledges financial support from the European Union within the FP7 framework (Marie Curie Intra-European Fellowship for Career Development). The authors thank Dr. Miri Kazes for providing the data shown in Figure 4a and Dr. Larissa Grinis for the HRTEM image shown in Figure 6a.

Keywords: electrochemistry · materials science · photochemistry · quantum dots · solar cells

[1] A. S. Brown, M. A. Green, *Phys. E* **2002**, *14*, 96 – 100.
[2] W. Shockley, H. J. Queisser, *J. Appl. Phys.* **1961**, *32*, 510 – 519.
[3] M. A. Green, K. Emery, Y. Hishikawa, W. Warta, *Prog. Photovoltaics* **2009**, *17*, 320 – 326.
[4] F. Remacle, C. P. Collier, G. Markovich, J. R. Heath, U. Banin, R. D. Levine, *J. Phys. Chem. B* **1998**, *102*, 7727 – 7734.
[5] N. V. Soloviev, A. Eichhofer, D. Fenske, U. Banin, *J. Am. Chem. Soc.* **2001**, *123*, 2354 – 2364.
[6] N. Tessler, V. Medvedev, M. Kazes, S. H. Kan, U. Banin, *Science* **2002**, *295*, 1506 – 1508.
[7] P. O. Anikeeva, J. E. Halpert, M. G. Bawendi, V. Bulovic, *Nano Lett.* **2009**, *9*, 2532 – 2536.
[8] E. V. Shevchenko, M. Ringler, A. Schwemer, D. V. Talapin, T. A. Klar, A. L. Rogach, J. Feldmann, A. P. Alivisatos, *J. Am. Chem. Soc.* **2008**, *130*, 3274 – 3275.
[9] L. Jdira, P. Liljeroth, E. Stoffels, D. Vanmaekelbergh, S. Speller, *Phys. Rev. B* **2006**, *73*, 115305.
[10] S. F. Wuister, A. v. Houselt, C. d. Mello Donegá, D. Vanmaekelbergh, A. Meijerink, *Angew. Chem.* **2004**, *116*, 3091 – 3095; *Angew. Chem. Int. Ed.* **2004**, *43*, 3029 – 3033.
[11] J. M. An, A. Franceschetti, S. V. Dudiy, A. Zunger, *Nano Lett.* **2006**, *6*, 2728 – 2735.
[12] E. Lifshitz, I. Dag, I. Litvin, G. Hodes, S. Gorer, R. Reisfeld, M. Zelner, H. Minti, *Chem. Phys. Lett.* **1998**, *288*, 188 – 196.
[13] A. L. Rogach, L. Katsikas, A. Kornowski, D. Su, A. Eychmüller, H. Weller, *Ber. Bunsen Phys. Chem.* **1996**, *100*, 1772 – 1778.
[14] A. L. Rogach, T. Franzl, T. A. Klar, J. Feldmann, N. Gaponik, V. Lesnyak, A. Shavel, A. Eychmüller, Y. P. Rakovich, J. F. Donegan, *J. Phys. Chem. C* **2007**, *111*, 14628 – 14637.
[15] T. Takagahara , K. Takeda, *Phys. Rev. B* **1992**, *46*, 15578 – 15581.
[16] S. Kan, T. Mokari, E. Rothenberg, U. Banin, *Nat. Mater.* **2003**, *2*, 155 – 158.
[17] R. Vogel, K. Pohl, H. Weller, *Chem. Phys. Lett.* **1990**, *174*, 241 – 246.
[18] R. Vogel, P. Hoyer, H. Weller, *J. Phys. Chem.* **1994**, *98*, 3183 – 3188.
[19] A. Zaban, O. I. Micic, B. A. Gregg, A. J. Nozik, *Langmuir* **1998**, *14*, 3153 – 3156.
[20] G. Hodes, A. Albu-Yaron, F. Decker, P. Motisuke, *Phys. Rev. B* **1987**, *36*, 4215 – 4221.
[21] S. Gorer, G. Hodes, *J. Phys. Chem.* **1994**, *98*, 5338 – 5346.
[22] S. Gorer, A. Albu-Yaron, G. Hodes, *J. Phys. Chem.* **1995**, *99*, 16442 – 16448.
[23] D. S. Ginger , N. C. Greenham, *Phys. Rev. B* **1999**, *59*, 10622 – 10629.
[24] N. C. Greenham, X. Peng, A. P. Alivisatos, *Phys. Rev. B* **1996**, *54*, 17628 – 17637.
[25] W. U. Huynh, J. J. Dittmer, A. P. Alivisatos, *Science* **2002**, *295*, 2425 – 2427.
[26] J. J. Choi, Y.-F. Lim, M. E. B. Santiago-Berrios, M. Oh, B.-R. Hyun, L. Sun, A. C. Bartnik, A. Goedhart, G. G. Malliaras, H. D. Abruna, F. W. Wise, T. Hanrath, *Nano Lett.* **2009**, *9*, 3749 – 3755.
[27] K. S. Leschkies, T. J. Beatty, M. S. Kang, D. J. Norris, E. S. Aydil, *ACS Nano* **2009**, *3*, 3638 – 3648.
[28] H. W. Hillhouse , M. C. Beard, *Curr. Opin. Colloid Interface Sci.* **2009**, *14*, 245 – 259.
[29] R. Loef, A. J. Houtepen, E. Talgorn, J. Schoonman, A. Goossens, *Nano Lett.* **2009**, *9*, 856 – 859.
[30] Z. Tachan, S. Rühle, A. Zaban, *Sol. Energy Mater. Sol. Cells* **2010**, *94*, 317 – 322.
[31] S. Rühle, S. Greenwald, E. Koren, A. Zaban, *Opt. Express* **2008**, *16*, 21801 – 21806.
[32] B. Weintraub, Y. Wei, Zhong L. Wang, *Angew. Chem.* **2009**, *121*, 9143 – 9147; *Angew. Chem. Int. Ed.* **2009**, *48*, 8981 – 8985.
[33] M. Toivola, M. Ferenets, P. Lund, A. Harlin, *Thin Solid Films* **2009**, *517*, 2799 – 2802.
[34] We note that some authors consider nanocomposite solar cells to be third-generation photovoltaics, while high-efficiency cells with conversion efficiencies beyond the Shockley–Queisser limit are termed fourth-generation photovoltaics.
[35] B. O'Regan , M. Grätzel, *Nature* **1991**, *353*, 737 – 740.
[36] I. Kaiser, K. Ernst, C.-H. Fischer, R. Könenkamp, C. Rost, I. Sieber, M. Lux-Steiner, *Sol. Energy Mater. Sol. Cells* **2001**, *67*, 89 – 96.
[37] S. Dor, T. Dittrich, A. Ofir, L. Grinis, A. Zaban, *J. Mater. Res.* **2008**, *23*, 975 – 980.
[38] A. Ofir, S. Dor, L. Grinis, A. Zaban, T. Dittrich, J. Bisquert, *J. Chem. Phys.* **2008**, *128*, 064703.
[39] S. Tirosh, T. Dittrich, A. Ofir, L. Grinis, A. Zaban, *J. Phys. Chem. B* **2006**, *110*, 16165 – 16168.
[40] P. R. F. Barnes, A. Y. Anderson, S. E. Koops, J. R. Durrant, B. C. O'Regan, *J. Phys. Chem. C* **2009**, *113*, 1126 – 1136.
[41] S. Soedergren, A. Hagfeldt, J. Olsson, S. E. Lindquist, *J. Phys. Chem.* **1994**, *98*, 5552 – 5556.
[42] G. Hodes, *J. Phys. Chem. C* **2008**, *112*, 17778 – 17787.
[43] J. Bisquert, G. Garcia-Belmonte, F. Fabregat-Santiago, *J. Solid State Electrochem.* **1999**, *3*, 337 – 347.
[44] K. Schwarzburg, F. Willig, *J. Phys. Chem. B* **1999**, *103*, 5743.
[45] F. Pichot, B. A. Gregg, *J. Phys. Chem. B* **2000**, *104*, 6.
[46] G. Kron, T. Egerter, J. H. Werner, U. Rau, *J. Phys. Chem. B* **2003**, *107*, 3556.
[47] G. Kron, U. Rau, J. H. Werner, *J. Phys. Chem. B* **2003**, *107*, 13258.
[48] B. A. Gregg, *J. Phys. Chem. B* **2003**, *107*, 13540.
[49] U. Rau, G. Kron, J. H. Werner, *J. Phys. Chem. B* **2003**, *107*, 13547.
[50] S. Rühle, D. Cahen, *J. Phys. Chem. B* **2004**, *108*, 17946 – 17951.
[51] S. Rühle, T. Dittrich, *J. Phys. Chem. B* **2005**, *109*, 9522 – 9526.
[52] G. Schlichthörl, S. Y. Huang, J. Sprague, A. J. Frank, *J. Phys. Chem. B* **1997**, *101*, 8141 – 8155.
[53] D. Cahen, G. Hodes, M. Grätzel, J. F. Guillemoles, I. Riess, *J. Phys. Chem. B* **2000**, *104*, 2053 – 2059.
[54] K. Zhu, E. A. Schiff, N. G. Park, J. van de Lagemaat, A. J. Frank, *Appl. Phys. Lett.* **2002**, *80*, 685 – 687.
[55] J. Xia, N. Masaki, K. Jiang, S. Yanagida, *J. Phys. Chem. C* **2007**, *111*, 8092 – 8097.
[56] S. Lee, J. H. Noh, H. S. Han, D. K. Yim, D. H. Kim, J.-K. Lee, J. Y. Kim, H. S. Jung, K. S. Hong, *J. Phys. Chem. C* **2009**, *113*, 6878 – 6882.
[57] J. Tornow, K. Schwarzburg, *J. Phys. Chem. C* **2007**, *111*, 8692 – 8698.
[58] H. Gerischer, *Electrochim. Acta* **1989**, *34*, 1005 – 1009.
[59] P. Chen, J. H. Yum, F. D. Angelis, E. Mosconi, S. Fantacci, S.-J. Moon, R. H. Baker, J. Ko, M. K. Nazeeruddin, M. Grätzel, *Nano Lett.* **2009**, *9*, 2487 – 2492.
[60] I. Gur, N. A. Fromer, M. L. Geier, A. P. Alivisatos, *Science* **2005**, *310*, 462 – 465.
[61] Y. Wu, C. Wadia, W. Ma, B. Sadtler, A. P. Alivisatos, *Nano Lett.* **2008**, *8*, 2551 – 2555.
[62] A. Luque, A. Marti, N. Lopez, E. Antolin, E. Canovas, C. Stanley, C. Farmer, L. J. Caballero, L. Cuadra, J. L. Balenzategui, *Appl. Phys. Lett.* **2005**, *87*, 083505.
[63] V. Popescu, G. Bester, M. C. Hanna, A. G. Norman, A. Zunger, *Phys. Rev. B* **2008**, *78*, 205321.
[64] N. G. Anderson, *J. Appl. Phys.* **1995**, *78*, 1850 – 1861.

[65] J. C. Rimada, L. Hernández, J. P. Connolly, K. W. J. Barnham, *Microelectr. J.* **2007**, *38*, 513 – 518.
[66] N. J. Ekins-Daukes, K. W. J. Barnham, J. P. Connolly, J. S. Roberts, J. C. Clark, G. Hill, M. Mazzer, *Appl. Phys. Lett.* **1999**, *75*, 4195 – 4197.
[67] K. W. J. Barnham, I. Ballard, J. P. Connolly, N. J. Ekins-Daukes, B. G. Kluftinger, J. Nelson, C. Rohr, *Phys. E* **2002**, *14*, 27 – 36.
[68] A. Franceschetti, J. M. An, A. Zunger, *Nano Lett.* **2006**, *6*, 2191 – 2195.
[69] M. T. Trinh, A. J. Houtepen, J. M. Schins, T. Hanrath, J. Piris, W. Knulst, A. P. L. M. Goossens, L. D. A. Siebbeles, *Nano Lett.* **2008**, *8*, 1713 – 1718.
[70] M. Dürr, A. Bamedi, A. Yasuda, G. Nelles, *Appl. Phys. Lett.* **2004**, *84*, 3397 – 3399.
[71] A. Luque, A. Martí, A. Bett, V. M. Andreev, C. Jaussaud, J. A. M. van Roosmalen, J. Alonso, A. Räuber, G. Strobl, W. Stolz, C. Algora, B. Bitnar, A. Gombert, C. Stanley, P. Wahnon, J. C. Conesa, W. G. J. H. M. van Sark, A. Meijerink, G. P. M. van Klink, K. Barnham, R. Danz, T. Meyer, I. Luque-Heredia, R. Kenny, C. Christofides, G. Sala, P. Benítez, *Sol. Energy Mater. Sol. Cells* **2005**, *87*, 467 – 479.
[72] N. S. Lewis, *Science* **2007**, *315*, 798 – 801.
[73] M. Mazzer, K. W. J. Barnham, I. M. Ballard, A. Bessiere, A. Ioannides, D. C. Johnson, M. C. Lynch, T. N. D. Tibbits, J. S. Roberts, G. Hill, C. Calder, *Thin Solid Films* **2006**, *511–512*, 76 – 83.
[74] G. Wei, S. R. Forrest, *Nano Lett.* **2007**, *7*, 218 – 222.
[75] R. D. Schaller, M. Sykora, J. M. Pietryga, V. I. Klimov, *Nano Lett.* **2006**, *6*, 424 – 429.
[76] A. J. Nozik, *Inorg. Chem.* **2005**, *44*, 6893 – 6899.
[77] A. J. Nozik, *Phys. E* **2002**, *14*, 115 – 120.
[78] A. J. Nozik, *Nat. Nanotechnol.* **2009**, *4*, 548 – 549.
[79] M. C. Beard, A. G. Midgett, M. Law, O. E. Semonin, R. J. Ellingson, A. J. Nozik, *Nano Lett.* **2009**, *9*, 836 – 845.
[80] H. Shpaisman, O. Niitsoo, I. Lubomirsky, D. Cahen, *Sol. Energy Mater. Sol. Cells* **2008**, *92*, 1541 – 1546.
[81] T. Trupke, P. Würfel, *J. Appl. Phys.* **2004**, *96*, 2347 – 2351.
[82] O. Niitsoo, S. K. Sarkar, C. Pejoux, S. Rühle, D. Cahen, G. Hodes, *J. Photochem. Photobiol. A* **2006**, *181*, 306 – 313.
[83] C.-H. Chang, Y.-L. Lee, *Appl. Phys. Lett.* **2007**, *91*, 053503.
[84] Y. L. Lee, C. H. Chang, *J. Power Sources* **2008**, *185*, 584 – 588.
[85] Y. Tak, S. J. Hong, J. S. Lee, K. Yong, *Cryst. Growth Des.* **2009**, *9*, 2627 – 2632.
[86] Y. F. Nicolau, M. Dupuy, M. Brunel, *J. Electrochem. Soc.* **1990**, *137*, 2915 – 2924.
[87] H. Lee, H. C. Leventis, S.-J. Moon, C. Peter, S. Ito, S. A. Haque, T. Torres, F. Nüesch, T. Geiger, S. M. Zakeeruddin, M. Grätzel, M. K. Nazeeruddin, *Adv. Funct. Mater.* **2009**, *19*, 2735 – 2742.
[88] T. Toyoda, J. Sato, Q. Shen, *Rev. Sci. Instrum.* **2003**, *74*, 297 – 299.
[89] H. J. Lee, P. Chen, S.-J. Moon, F. Sauvage, K. Sivula, T. Bessho, D. R. Gamelin, P. Comte, S. M. Zakeeruddin, S. I. Seok, M. Grätzel, M. K. Nazeeruddin, *Langmuir* **2009**, *25*, 7602 – 7608.
[90] D. R. Baker, P. V. Kamat, *J. Phys. Chem. C* **2009**, *113*, 17967 – 17972.
[91] D. R. Baker, P. V. Kamat, *Adv. Funct. Mater.* **2009**, *19*, 805 – 811.
[92] S. Hotchandani, P. V. Kamat, *Chem. Phys. Lett.* **1992**, *191*, 320 – 326.
[93] Y. Tak, S. J. Hong, J. S. Lee, K. Yong, *J. Mater. Chem.* **2009**, *19*, 5945 – 5951.
[94] W. Lee, S. K. Min, V. Dhas, S. B. Ogale, S. H. Han, *Electrochem. Commun.* **2009**, *11*, 103 – 106.
[95] C. Nasr, S. Hotchandani, W. Y. Kim, R. H. Schmehl, P. V. Kamat, *J. Phys. Chem. B* **1997**, *101*, 7480 – 7487.
[96] Y. J. Shen, Y. L. Lee, *Nanotechnology* **2008**, *19*, 045602.
[97] R. S. Dibbell, D. F. Watson, *J. Phys. Chem. C* **2009**, *113*, 3139 – 3149.
[98] L. M. Peter, D. J. Riley, E. J. Tull, K. G. U. Wijayantha, *Chem. Commun.* **2002**, 1030 – 1031.
[99] N. Guijarro, T. Lana-Villarreal, I. Mora-Sero, J. Bisquert, R. Gomez, *J. Phys. Chem. C* **2009**, *113*, 4208 – 4214.
[100] Q. Shen, J. Kobayashi, L. J. Diguna, T. Toyoda, *J. Appl. Phys.* **2008**, *103*, 084304.
[101] L. J. Diguna, Q. Shen, J. Kobayashi, T. Toyoda, *Appl. Phys. Lett.* **2007**, *91*, 023116.
[102] Y. L. Lee, B. M. Huang, H. T. Chien, *Chem. Mater.* **2008**, *20*, 6903 – 6905.
[103] H. Lee, M. Wang, P. Chen, D. R. Gamelin, S. M. Zakeeruddin, M. Grätzel, M. K. Nazeeruddin, *Nano Lett.* **2009**, *9*, 4221 – 4227.
[104] I. Mora-Seró, S. Giménez, T. Moehl, F. Fabregat-Santiago, T. Lana-Villareal, R. Gómez, J. Bisquert, *Nanotechnology* **2008**, *19*, 424007.
[105] J. Chen, J. L. Song, X. W. Sun, W. Q. Deng, C. Y. Jiang, W. Lei, J. H. Huang, R. S. Liu, *Appl. Phys. Lett.* **2009**, *94*, 153115.
[106] I. Robel, V. Subramanian, M. Kuno, P. V. Kamat, *J. Am. Chem. Soc.* **2006**, *128*, 2385 – 2393.
[107] J. H. Bang, P. V. Kamat, *ACS Nano* **2009**, *3*, 1467 – 1476.
[108] P. V. Kamat, *J. Phys. Chem. C* **2008**, *112*, 18737 – 18753.
[109] J. Chen, D. W. Zhao, J. L. Song, X. W. Sun, W. Q. Deng, X. W. Liu, W. Lei, *Electrochem. Commun.* **2009**, *11*, 2265 – 2267.
[110] P. K. Singh, K. W. Kim, H. W. Rhee, *Electrochem. Commun.* **2009**, *11*, 1247 – 1250.
[111] J. R. Mann, D. F. Watson, *Langmuir* **2007**, *23*, 10924 – 10928.
[112] A. Kongkanand, K. Tvrdy, K. Takechi, M. Kuno, P. V. Kamat, *J. Am. Chem. Soc.* **2008**, *130*, 4007 – 4015.
[113] S. Giménez, I. Mora-Seró, L. Macor, N. Guijarro, T. Lana-Villarreal, R. Gómez, L. J. Diguna, Q. Shen, T. Toyoda, J. Bisquert, *Nanotechnology* **2009**, *20*, 295204.
[114] B. Carlson, K. Leschkies, E. S. Aydil, X. Y. Zhu, *J. Phys. Chem. C* **2008**, *112*, 8419 – 8423.
[115] J. Chen, C. Li, J. L. Song, X. W. Sun, W. Lei, W. Q. Deng, *Appl. Surf. Sci.* **2009**, *255*, 7508 – 7511.
[116] K. S. Leschkies, R. Divakar, J. Basu, E. Enache-Pommer, J. E. Boercker, C. B. Carter, U. R. Kortshagen, D. J. Norris, E. S. Aydil, *Nano Lett.* **2007**, *7*, 1793 – 1798.
[117] B. Farrow, P. V. Kamat, *J. Am. Chem. Soc.* **2009**, *131*, 11124 – 11131.
[118] X.-F. Gao, H.-B. Li, W.-T. Sun, Q. Chen, F.-Q. Tang, L.-M. Peng, *J. Phys. Chem. C* **2009**, *113*, 7531 – 7535.
[119] X. B. Cao, P. Chen, Y. Guo, *J. Phys. Chem. C* **2008**, *112*, 20560 – 20566.
[120] P. Yu, K. Zhu, A. G. Norman, S. Ferrere, A. J. Frank, A. J. Nozik, *J. Phys. Chem. B* **2006**, *110*, 25451 – 25454.
[121] R. Plass, S. Pelet, J. Krueger, M. Grätzel, U. Bach, *J. Phys. Chem. B* **2002**, *106*, 7578 – 7580.
[122] B.-R. Hyun, Y.-W. Zhong, A. C. Bartnik, L. Sun, H. D. Abruña, F. W. Wise, J. D. Goodreau, J. R. Matthews, T. M. Leslie, N. F. Borrelli, *ACS Nano* **2008**, *2*, 2206 – 2212.
[123] C. Ratanatawanate, Y. Tao, K. J. Balkus, *J. Phys. Chem. C* **2009**, *113*, 10755 – 10760.
[124] K. S. Leschkies, A. G. Jacobs, D. J. Norris, E. S. Aydil, *Appl. Phys. Lett.* **2009**, *95*, 193103.
[125] K. T. Kuo, D. M. Liu, S. Y. Chen, C. C. Lin, *J. Mater. Chem.* **2009**, *19*, 6780 – 6788.
[126] K. G. U. Wijayantha, L. M. Peter, L. C. Otley, *Sol. Energy Mater. Sol. Cells* **2004**, *83*, 363 – 369.
[127] S. Ito, T. N. Murakami, P. Comte, P. Liska, C. Grätzel, M. K. Nazeeruddin, M. Grätzel, *Thin Solid Films* **2008**, *516*, 4613 – 4619.
[128] L. Grinis, S. Dor, A. Ofir, A. Zaban, *J. Photochem. Photobiol. A* **2008**, *198*, 52 – 59.
[129] S. Dor, S. Rühle, A. Ofir, M. Adler, L. Grinis, A. Zaban, *Colloids Surf. A* **2009**, *342*, 70 – 75.
[130] C. J. Barbé, F. Arendse, P. Comte, M. Jirousek, F. Lenzmann, V. Shklover, M. Grätzel, *J. Am. Ceram. Soc.* **1997**, *80*, 3157 – 3171.
[131] X. Feng, K. Shankar, O. K. Varghese, M. Paulose, T. J. Latempa, C. A. Grimes, *Nano Lett.* **2008**, *8*, 3781 – 3786.
[132] B. Cao, W. Cai, Y. Li, F. Sun, L. Zhang, *Nanotechnology* **2005**, *16*, 1734.
[133] R. Tena-Zaera, J. Elias, G. Wang, C. Levy-Clement, *J. Phys. Chem. C* **2007**, *111*, 16706 – 16711.
[134] M. J. Zheng, L. D. Zhang, G. H. Li, W. Z. Shen, *Chem. Phys. Lett.* **2002**, *363*, 123 – 128.
[135] M. Krunks, T. Dedova, I. O. Açik, *Thin Solid Films* **2006**, *515*, 1157 – 1160.
[136] A. B. F. Martinson, T. W. Hamann, M. J. Pellin, J. T. Hupp, *Chem. Eur. J.* **2008**, *14*, 4458 – 4467.
[137] L. Grinis, A. Ofir, S. Dor, S. Yahav, A. Zaban, *Isr. J. Chem.* **2008**, *48*, 269 – 275.
[138] C. S. Lao, P. X. Gao, R. S. Yang, Y. Zhang, Y. Dai, Z. L. Wang, *Chem. Phys. Lett.* **2006**, *417*, 358 – 362.
[139] Z.-H. Liang, Y.-J. Zhu, G.-F. Cheng, Y.-H. Huang, *J. Mater. Sci.* **2007**, *42*, 477 – 482.
[140] P. X. Gao, Y. Ding, W. Mai, W. L. Hughes, C. Lao, Z. L. Wang, *Science* **2005**, *309*, 1700 – 1704.
[141] V. G. Pol, A. Zaban, *J. Phys. Chem. C* **2007**, *111*, 14574 – 14578.
[142] Y. Tachibana, H. Y. Akiyama, Y. Ohtsuka, T. Torimoto, S. Kuwabata, *Chem. Lett.* **2007**, *36*, 88 – 89.

[143] H. J. Lee, J.-H. Yum, H. C. Leventis, S. M. Zakeeruddin, S. A. Haque, P. Chen, S. I. Seok, M. Grätzel, M. K. Nazeeruddin, *J. Phys. Chem. C* **2008**, *112*, 11600 – 11608.
[144] Y.-L. Lee , Y.-S. Lo, *Adv. Funct. Mater.* **2009**, *19*, 604 – 609.
[145] G. Hodes, J. Manassen, D. Cahen, *J. Electrochem. Soc.* **1980**, *127*, 544 – 549.
[146] M. Shalom, S. Dor, S. Rühle, L. Grinis, A. Zaban, *J. Phys. Chem. C* **2009**, *113*, 3895 – 3898.
[147] S.-C. Lin, Y.-L. Lee, C.-H. Chang, Y.-J. Shen, Y.-M. Yang, *Appl. Phys. Lett.* **2007**, *90*, 143517.
[148] Y. Tachibana, K. Umekita, Y. Otsuka, S. Kuwabata, *J. Phys. D* **2008**, *41*, 102002.
[149] G. Larramona, C. Chone, A. Jacob, D. Sakakura, B. Delatouche, D. Pere, X. Cieren, M. Nagino, R. Bayon, *Chem. Mater.* **2006**, *18*, 1688 – 1696.
[150] M. Grätzel, U. Bach, D. Lupo, P. Comte, J. E. Moser, F. Weissortel, J. Salbeck, H. Spreitzer, *Nature* **1998**, *395*, 583 – 585.
[151] H. J. Snaith, M. Grätzel, *Adv. Mater.* **2007**, *19*, 3643 – 3647.
[152] J.-H. Yum, P. Chen, M. Grätzel, M. K. Nazeeruddin, *ChemSusChem* **2008**, *1*, 699 – 707.
[153] H. J. Snaith, L. Schmidt-Mende, *Adv. Mater.* **2007**, *19*, 3187 – 3200.
[154] M. Wang, C. Grätzel, S.-J. Moon, R. Humphry-Baker, N. Rossier-Iten, S. M. Zakeeruddin, M. Grätzel, *Adv. Funct. Mater.* **2009**, *19*, 2163 – 2172.
[155] B. Mahrov, A. Hagfeldt, F. Lenzmann, G. Boschloo, *Sol. Energy Mater. Sol. Cells* **2005**, *88*, 351 – 362.
[156] I. K. Ding, N. Tétreault, J. Brillet, B. E. Hardin, E. H. Smith, S. J. Rosenthal, F. Sauvage, M. Grätzel, M. D. McGehee, *Adv. Funct. Mater.* **2009**, *19*, 2431 – 2436.
[157] V. P. S. Perera, K. Tennakone, *Sol. Energy Mater. Sol. Cells* **2003**, *79*, 249 – 255.
[158] K. Tennakone, G. K. R. Senadeera, D. B. R. A. De Silva, I. R. M. Kottegoda, *Appl. Phys. Lett.* **2000**, *77*, 2367 – 2369.
[159] J. Xia, N. Masaki, M. Lira-Cantu, Y. Kim, K. Jiang, S. Yanagida, *J. Phys. Chem. C* **2008**, *112*, 11569 – 11574.
[160] C. Lévy-Clément, R. Tena-Zaera, M. A. Ryan, A. Katty, G. Hodes, *Adv. Mater.* **2005**, *17*, 1512 – 1515.
[161] A. Belaidi, T. Dittrich, D. Kieven, J. Tornow, K. Schwarzburg, M. Lux-Steiner, *Phys. Status Solidi R* **2008**, *2*, 172 – 174.
[162] T. Dittrich, D. Kieven, M. Rusu, A. Belaidi, J. Tornow, K. Schwarzburg, M. Lux-Steiner, *Appl. Phys. Lett.* **2008**, *93*, 053113.
[163] Y. Itzhaik, O. Niitsoo, M. Page, G. Hodes, *J. Phys. Chem. C* **2009**, *113*, 4254 – 4256.
[164] M. Page, O. Niitsoo, Y. Itzhaik, D. Cahen, G. Hodes, *Energy Environ. Sci.* **2009**, *2*, 220 – 223.
[165] L. Grinis, S. Kotlyar, S. Rühle, J. Grinblat, A. Zaban, *Adv. Funct. Mater.* **2010**, *20*, 282 – 288.
[166] Y. Diamant, S. G. Chen, O. Melamed, A. Zaban, *J. Phys. Chem. B* **2003**, *107*, 1977 – 1981.
[167] I. Mora-Seró, S. Giménez, F. Fabregat-Santiago, R. Gómez, Q. Shen, T. Toyoda, J. Bisquert, *Acc. Chem. Res.* **2009**, *42*, 1848 – 1857.
[168] S. Rühle, M. Greenshtein, S. G. Chen, A. Merson, H. Pizem, C. S. Sukenik, D. Cahen, A. Zaban, *J. Phys. Chem. B* **2005**, *109*, 18907 – 18913.
[169] Z. P. Zhang, S. M. Zakeeruddin, B. C. O'Regan, R. Humphry-Baker, M. Grätzel, *J. Phys. Chem. B* **2005**, *109*, 21818 – 21824.
[170] N. Kopidakis, N. R. Neale, A. J. Frank, *J. Phys. Chem. B* **2006**, *110*, 12485 – 12489.
[171] Y. Liu, A. Hagfeldt, X. R. Xiao, S. E. Lindquist, *Sol. Energy Mater. Sol. Cells* **1998**, *55*, 267 – 281.
[172] Z.-S. Wang, G. Zhou, *J. Phys. Chem. C* **2009**, *113*, 15417 – 15421.
[173] M. Soreni-Harari, N. Yaacobi-Gross, D. Steiner, A. Aharoni, U. Banin, O. Millo, N. Tessler, *Nano Lett.* **2008**, *8*, 678 – 684.
[174] P. V. Kamat, *J. Phys. Chem. C* **2007**, *111*, 2834 – 2860.
[175] M. Shalom, S. Rühle, I. Hod, S. Yahav, A. Zaban, *J. Am. Chem. Soc.* **2009**, *131*, 9876 – 9877.
[176] H. J. Snaith, *Adv. Funct. Mater.* **2010**, *20*, 13 – 19.

Received: January 27, 2010
Published online on July 14, 2010

